

Sub-surface modifications in silicon with ultra-short pulsed lasers above 2 microns

Roland A. Richter,¹ Nikolai Tolstik,^{1,2} Sebastien Rigaud,¹ Paul Dalla Valle,¹ Andreas Erbe,³ Petra Ebbinghaus,⁴ Ignas Astrauskas,⁵ Vladimir Kalashnikov,^{5,6} Evgeni Sorokin,⁵ and Irina T. Sorokina^{1,2,*}

¹*Department of Physics, NTNU, Norwegian University of Science and Technology, Trondheim, Norway*

²*ATLA Lasers AS*

³*Department of Materials Science and Engineering, NTNU,*

Norwegian University of Science and Technology, Trondheim, Norway

⁴*Max-Planck-Institut für Eisenforschung GmbH, Düsseldorf, Germany*

⁵*Photonics Institute, Vienna University of Technology, Vienna, Austria*

⁶*Dipartimento di Ingegneria dell'Informazione, Sapienza University of Rome, Italy*

Nonlinear optical phenomena in silicon such as self-focusing and multi-photon absorption are strongly dependent on the wavelength, energy and duration of the exciting pulse. Thus, a pronounced wavelength dependence of the sub-surface modifications with ultra-short pulsed lasers exists, especially for wavelengths $>2 \mu\text{m}$. This wavelength dependence is investigated for wavelengths in the range of 1950-2400 nm, at a pulse duration between 0.5-10 ps and the pulse energy varying from 1 μJ to 1 mJ. Numerical and experimental analyses have been performed on both the surface and sub-surface of Si wafers processed with fibre-based lasers built in-house that operate in this wavelength range. The results have been compared to the literature data at 1550 nm. The analysis carried out has shown that due to a dip in the nonlinear absorption spectrum and a peak in the spectrum of the third-order non-linearity, the wavelengths between 2000-2200 nm are more favourable for creating sub-surface modifications in silicon. This is the case even though those wavelengths do not allow as tight a focusing as those at 1550 nm in the linear regime. This problem is compensated by an increased self-focusing due to the nonlinear Kerr-effect around 2100 nm at high light intensities, characteristic for ultra-short pulses.

I. INTRODUCTION AND STATE-OF-THE-ART

Silicon wafers are currently largely separated from the bulk mono-crystalline Si-block using thin diamond saws, which introduces a loss of material of up to 50 % [1]. For extremely thin wafers with a thickness $\leq 100 \mu\text{m}$ the loss increases to 70 % [1]. Thus, alternative methods for wafer separation are in development, such as epitaxial Si lift-off, stress-induced spalling, and smart-cut [2, 3]. This latter technique employs the fact that by the introduction of defects in a target layer below the Si wafer surface this layer will be weakened, allowing the wafer itself to be removed. There are multiple techniques for introducing such defects into bulk Si. The expansion coefficient difference for two materials can be used [4], without adding modifications inside the crystal. However, the crystal itself can be modified internally by the use of a layer of porous Si [5], the use of high-energy protons [3] or the use of two-photon absorption of laser pulses at 1550 nm [6].

Even though much work has been conducted at common wavelengths such as 1064 nm and 1550 nm, both experimentally and numerically [7–14] only a small amount of work has been done at longer wavelengths, including 1965 nm [10], 1970 nm [15] and 2300 nm [10, 16]. Chambonneau et al. [15] used a Tm-fiber laser for generating pulses with a duration of 400 ps, which then were compressed outside of the fiber laser. Furthermore, they investigated the number of pulses necessary to modify silicon, depending on the pulse energy. In the latter work a femtosecond

OPO (optical parametric oscillator) was used to produce modifications below a SiO_2 layer, but not within bulk Si.

In the first section of the present paper we numerically investigate the influence of the wavelength, pulse energy and pulse duration on the defect formation of silicon using both numerical simulations and experiments for wavelengths between 1950-2400 nm. The results obtained are compared with the existing data for 1550 nm, 1970 nm and 2300 nm. Thereby we can confirm the preliminary results we showed in [10], that an optimal wavelength range for silicon processing exists.

On the experimental side, this paper is separated into two separate parts. In those parts several different lasers have been used to modify a Si-crystal both on the surface and within the bulk material by using the wavelengths longer than 1950 nm. In order to optimize the process both in quality and speed, several parameters such as pulse energy, pulse duration and wavelength had to be optimized. It has been already demonstrated that shorter pulses provide better cut quality and precision compared to longer pulses [17, 18], while lowering the ablation threshold. We have previously shown that longer wavelengths in the mid-infrared range between 2000 nm and 2200 nm are beneficial for processing of bulk Si [10]. This is due to the combination of lower non-linear absorption [19] and higher self-focusing [20]. Therefore, we present results showing the creation of sub-surface modifications within silicon by using pulses at nano-joule levels at two different wavelengths (1965 nm and 2350 nm) in the first sub-part of the experimental section of this paper. Afterwards, we present the generation of sub-surface modifications in silicon using micro-joule level pulses at

* sorokina@ntnu.no

a wavelength of 2090 nm in the second sub-part.

In summary we present here for to our knowledge the first time the results of both numerical and experimental studies above 1550 nm using fiber based lasers with a wavelength of 1965 nm, 2090 nm and 2350 nm at different pulse energies. The results show not only that silicon processing is favourable at longer wavelengths (as it was shown before in previous studies [10, 15]), but also that an optimum wavelength range for modifying silicon exists. This is based on the wavelength dependencies of the non-linear refractive index n_2 and the multi-photon absorption coefficients β and γ for two- and three-photon absorption, respectively.

II. METHODOLOGY

The spectrum of the non-linear multi-photon absorption calculated (in our case) as a sum of the two-photon- and three-photon-absorption has a “dip” within the wavelength range we target (between 2000-2200 nm), as shown in [10]. The values for two-photon-absorption decrease above ≈ 1800 nm, while the three-photon-absorption is noticeably rising above 2300 nm, thus leaving a gap in between [10, 11].

The Nonlinear Figure of Merit (NFoM) characterizing the relative merit of the Kerr nonlinearity coefficient versus the two-photon nonlinearity is usually defined as the ratio between both values, divided by the optical wavelength in vacuum [21]. Extending this expression to multi-photon absorption results in the NFoM that is written in the following form [20]:

$$NFOM = \sum_K \frac{n_2(\lambda)}{\lambda \beta^{(K)} I^{(K-1)}} \quad (1)$$

with λ the wavelength in vacuum, $n_2(\lambda)$ the wavelength-dependent refractive index, I the field intensity and $\beta^{(K)}$ the coefficient for K -photon absorption.

Based on Equation (1), an optimal wavelength range for generating sub-surface modifications could be estimated to be in the range of 2000-2300 nm [10]. The exact wavelength depends on the exact value of the material parameters involved, such as the value for the wavelength-dependent Kerr-nonlinearity $n_2(\lambda)$, which again depends on the material properties (e.g. single-crystal versus polycrystalline material, n-doped versus p-doped). This explains a large range of the reported values of silicon nonlinearities, including measurement errors up to 30 % [19, 20]. Thus, one can only predict a certain wavelength range, not an exact value of the optimal wavelength for generating sub-surface modifications.

To model the propagation of the pulse through the

material, we use the non-linear Schrödinger equation [11]

$$\begin{aligned} \partial_z E = & \frac{i}{2k_0} \Delta E + \frac{ik_0 n_2}{n_0} |E|^2 E \\ & - \frac{1}{2} \sum_K \beta^{(K)} |E|^{2K-2} E \\ & - \frac{\sigma}{2} (1 + i\omega_0 \tau_c) N E \end{aligned} \quad (2)$$

Equation (2) describes the propagation of a time (t)-dependent and transversely inhomogeneous laser field E through bulk Si along the z -axis. The diffraction is taken into account by the transverse Laplacian, where k_0 is the wavenumber. The nonlinear effects of self-phase modulation and self-focusing are described by the term proportional to n_2 , and $\tau_c = 3.5$ fs is the free-carriers momentum scattering time [11]. The non-linear multi-photon absorption for K -photon-absorption ($\beta^{(K)}$), the absorption caused by free carriers with the concentration N , and the inverse bremsstrahlung absorption σ are taken into account, as well. Since the investigated wavelengths are in the range where the single-photon-absorption and higher-photon-absorption could be neglected [22], we have considered the action of only two- and three-photon absorption. The numerical simulation was done while using support functions from the library deal.II [23].

The paraxial approximation introduces several simplifications into the beam propagation equation, but is only valid until a certain beam diameter [24]. Thus, if the beam is focused too strongly because of the optical Kerr-effect, Equation (2) which uses that approximation loses its' validity. Deviations from paraxiality also have to be taken into account when simulating lenses with extremely high NA.

There are different approaches for calculating the response of the material if irradiated with ultra-short pulses, which are extensively discussed in [25]. Examples include the two-temperature-model (TTM) and its extension, the three-temperature model [26], a hydrodynamic approach and molecular dynamics (MD) simulations. Furthermore, hybrid models such as a combination of a TTM and a MD are suggested [25]. In order to simplify calculations, in this study we take into account only the generated carrier density. This value can be calculated by using [11]:

$$\partial_t N = \sum_K \frac{\beta^{(K)} |E|^{2K}}{K \hbar \omega_0} \quad (3)$$

where $|E|^2 \equiv I$.

III. NUMERICAL SIMULATIONS

An initial rough comparison of the action produced on silicon by ultra-short pulses at different wavelengths can be done using Equation (2), by comparing the transported energy towards the focal spot. The results of such simulations for the wavelengths 1550 nm, 1950 nm, 2150 nm and

2350 nm with a pulse energy of 1 μJ , 10 μJ and 100 μJ for two different values of n_2 [19, 20] are shown in Figure 1. The results denoted with “high n_2 -values” and “low n_2 -values” use n_2 -values taken from [20] and [19], respectively. The pulse duration is set to 5 ps, to correlate as close as possible with the experiments presented in Section IV. In these experiments, a large range of different lenses and focal depths was used. To limit the presented data to a reasonable amount, while still being able to demonstrate representative results, in the simulations we selected a lens with a focal length of 8 mm. The beam radius was adjusted to have a comparable focal spot area for linear focusing, with a beam radius of 1 mm for the wavelength of 1550 nm.

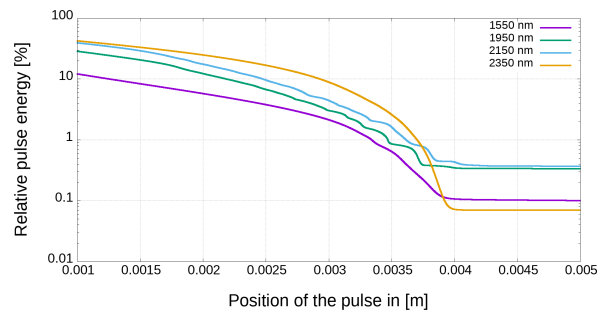
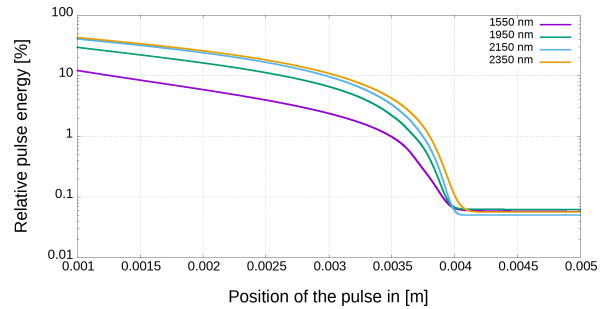
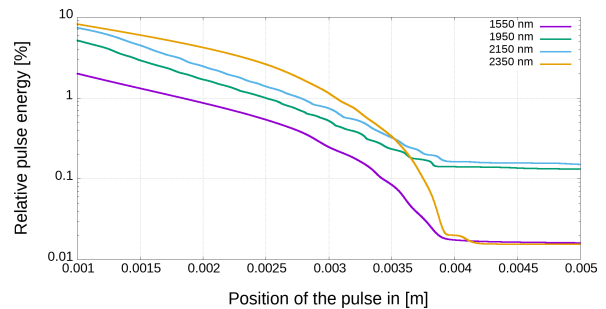
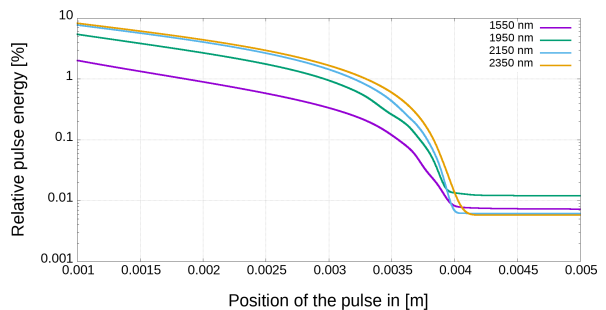
While the pulse with the shortest wavelength is absorbed quite significantly already on the way to the focal spot, the other wavelengths can retain more energy, before depositing it closer to the focal spot. In addition, the absorption close to reaching the focal spot depends on the value of the third-order non-linearity, as shown e.g. when comparing Figure 1a and Figure 1b. Here one also can see the ripples, originating from the strong self-focusing within the material, followed by local absorption and collapse, which show up in Figures 2 and 3, too.

In the Figures 1a to 1f most of the pulse energy is absorbed already in the first millimeter of the material, leading to a loss of 50-99% of the pulse energy, depending on the initial pulse energy and wavelength. This process is independent of the value of the Kerr-nonlinearity. This high loss also means that the pulse has $\approx 0.5 \mu\text{J}$ left for 1 μJ initial pulse energy, $\approx 0.9 \mu\text{J}$ is left for 10 μJ initial pulse energy and $\approx 0.9 \mu\text{J}$ is left for 100 μJ initial pulse energy, which in turn shows that an increase of the pulse energy does not necessarily increase the energy transported to the focal spot, but instead increases the chance of damaging material on the way to the focal spot. Due to the similarity of the transported energy for the pulse with 10 μJ and with 100 μJ the profile for the generated intensity and carriers are very similar. Thus, those figures are omitted in Figure 2 and Figure 3.

When considering the achieved intensities, one can see in Figure 2 both the effect of the nonlinear refractive index and the collapse of the pulse.

In Figure 2 the self-focusing of the pulse at a wavelength of 1950 nm and 2150 nm starts at a significantly smaller depth than for the other two wavelengths. Self-focusing at a smaller depth leads to a modification zone which is spread out much more, compared to a pulse which is focused at a larger depth.

The achieved intensity for the shortest wavelength (1550 nm) is higher than for other wavelengths when assuming the lowest reported values for the Kerr-effect in silicon, even though – as it is shown in Figure 1 – a much lower portion of the pulse energy is transported to the focal spot for this wavelength. This can be explained by the interplay of stronger focusing at shorter wavelengths, something which is compensated for the longer wavelengths with an increasing Kerr-effect around 2-2.2 μm

(a) High n_2 -values, 1 μJ pulse energy(b) Low n_2 -values, 1 μJ pulse energy(c) High n_2 -values, 10 μJ pulse energy(d) Low n_2 -values, 10 μJ pulse energy

and thus even tighter focusing.

Finally, the effect already manifested in Figure 1 also shows up in the intensity curves: Since most of the energy of the pulse is absorbed in the first small part of the beam path, the resulting energy at the focal spot is approximately the same for 10 and 100 μJ , being only

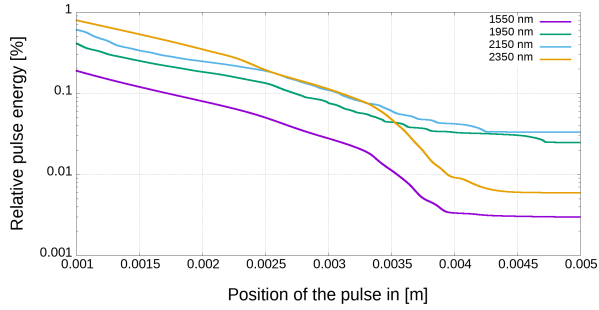
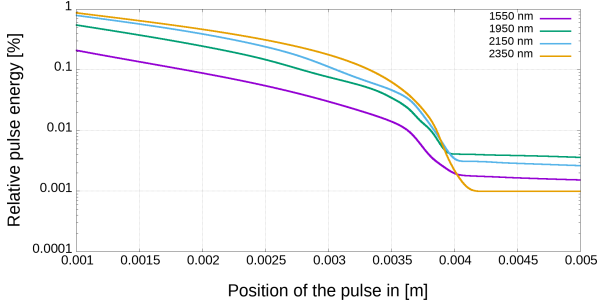
(e) High n_2 -values, 100 μJ pulse energy(f) Low n_2 -values, 100 μJ pulse energy

FIG. 1: Energy of a pulse with different wavelengths and energies, depending on the position within the material. The focal length of the used lens is $f = 8$ mm, with the focal point at $f_i = 4$ mm inside the material. The pulse duration is 5 ps, and the pulse energy is varied between 1 μJ and 100 μJ .

slightly higher than that for 1 μJ . This results in the same intensity levels for the former two, and only slightly lower intensity levels for the latter one. Higher intensity also means higher absorption, which can be calculated using [11]

$$\partial_t I = \sum_K \beta^{(K)} I^K + \sigma N I \quad (4)$$

Here, the absorption does not only depend on the non-linear absorption, but also on the free carrier density, which in turn is increased by the pulse itself (see Equation (3)). This generated free-carrier density is shown in Figure 3, both for low and high n_2 -values.

Again, the pulse at 1950 nm and 2150 nm can generate more free carriers, compared to the other two wavelengths, which in turn increases absorption and diffraction. This also holds true when considering the lower Kerr-nonlinearity. Even though the shortest wavelength could generate the highest intensity, the amount of the generated free carriers is approximately the same for all wavelengths, because of the higher free-carrier-generation efficiency at longer wavelengths.

Moreover, because of the similar intensities for all pulse energies, the generated free carrier densities are also at

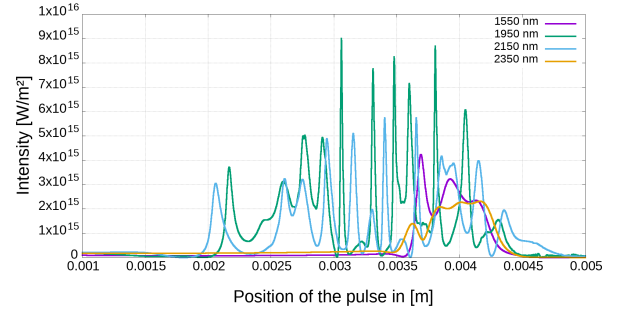
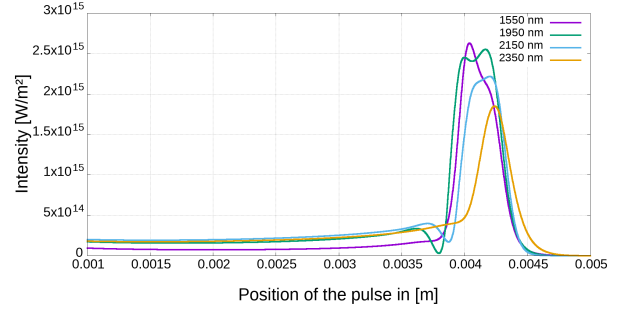
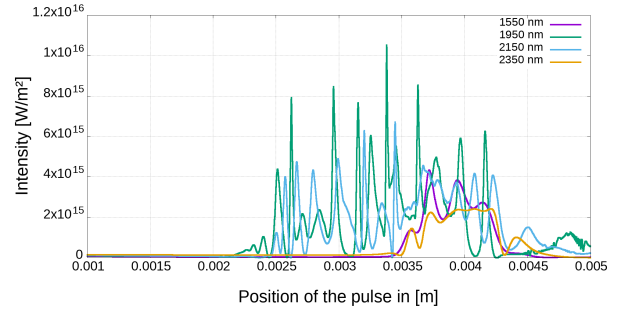
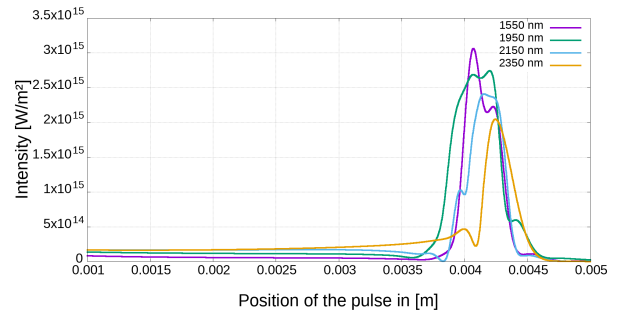
(a) High n_2 -values, 1 μJ pulse energy(b) Low n_2 -values, 1 μJ pulse energy(c) High n_2 -values, 10 μJ pulse energy(d) Low n_2 -values, 10 μJ pulse energy

FIG. 2: Intensity of a pulse with different wavelengths and energies, depending on the position within the material. The focal length of the used lens is $f = 8$ mm, with the focal point at $f_i = 4$ mm inside the material. The pulse duration is 5 ps, and the pulse energy is varied between 1 μJ and 10 μJ .

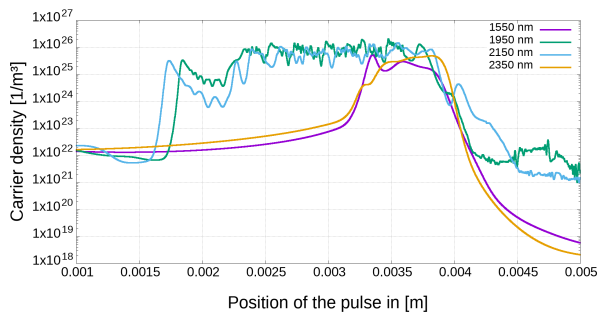
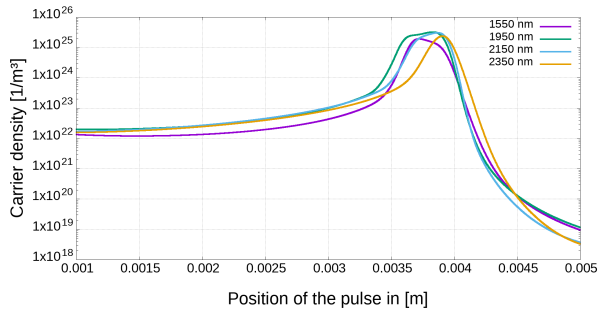
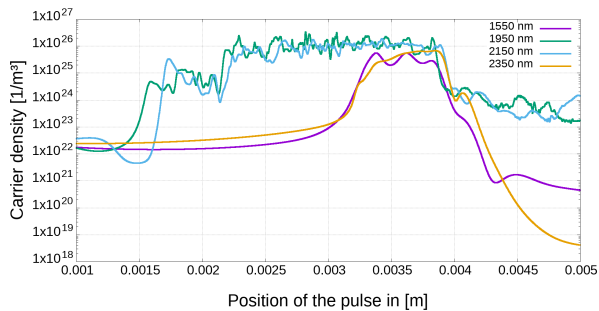
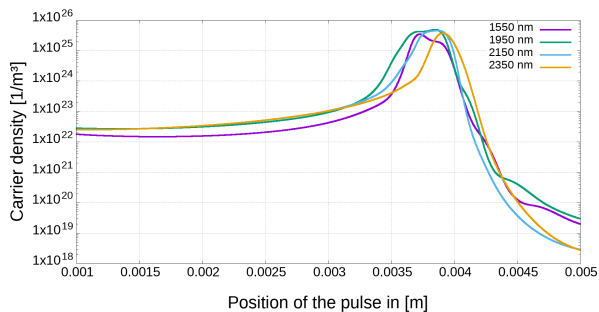
(a) High n_2 -values, 1 μJ pulse energy(b) Low n_2 -values, 1 μJ pulse energy(c) High n_2 -values, 10 μJ pulse energy(d) Low n_2 -values, 10 μJ pulse energy

FIG. 3: Generated free carrier density from a pulse with different wavelengths, depending on the position within the material. The focal length of the used lens is $f = 8$ mm, with the focal point at $f_i = 4$ mm inside the material. The pulse duration is 5 ps, and the pulse energy is varying between 1 μJ and 10 μJ .

approximately the same level, thereby confirming again that increasing the pulse energy from 10 μJ to 100 μJ does not increase modifications, but rather hinders them by destroying the material on the way to the focal spot.

When considering extended models, such as Two Temperature Models (TTM) as for example in [9] and [13], the free carrier density also plays an important role by coupling the energy of the generated free carriers to the lattice itself by the coupling constant [9]

$$\gamma(N) = \frac{3k_B N}{\tau_0 \left(1 + \left(\frac{N}{N_{crit}}\right)^2\right)} \quad (5)$$

Thus, a higher free carrier density makes the energy transfer from the excited carriers to the lattice more efficient. This assumption must be still investigated further by coupling the pulse propagation to a two-temperature model. Finally, two different processes can lead to melting [27, 28]. On the one hand, the carrier density can be increased up to a critical carrier density [13, 29]. At that density, enough free carriers are excited that the material can show non-thermal melting [18, 28, 30, 31]. This critical density ($n_c \approx 1 \times 10^{22} \text{ cm}^{-3} \equiv 1 \times 10^{28} \text{ m}^{-3}$ [29]) is reached when approximately 10-20% of the valence electrons are excited. This state shows a behaviour similar to melting, while the lattice temperature is still below the melting temperature. The other process is conventional thermal melting, when the lattice reaches a temperature above the melting temperature.

Based on the numerical simulation data shown above (Figures 1 to 3) we can conclude that the created modifications in Si using the lens with $f = 8$ mm and $f_i = 4$ mm have a thermal nature, since the generated free-carrier density did not exceed the critical density.

Our numerical simulations also confirm the initial assumption, that the wavelengths in the range of 2000-2200 nm are more efficient for modifying Si compared to wavelengths above 2200 nm and below 1900 nm.

IV. EXPERIMENTAL

A. Laser sources

In order to get experimental data which can be used as verification of the numerical results, modifications on and below the surface of Si-wafers were made using three different home-built lasers based on specialty fibers: An all-fiber LMA-based MOPA (Master Oscillator, Power Amplifier) system based on Tm operating at a central wavelength of $\lambda = 2100$ nm, $\tau_p = 2$ ps and $W_{max} = 980$ nJ (see Section IV A 1), a fibre-based Ho-CPA laser operating at $\lambda = 2090$ nm, $\tau_p = 5$ ps and $W_{max} = 760$ μJ (see Section IV A 2) and an Er-fiber based Cr:ZnS laser operating at $\lambda = 2350$ nm, $\tau_p = 1.7$ ps and $W_{max} = 20.3$ nJ (see Section IV A 3).

1. Tm-based fibre MOPA, operating at $\lambda = 2\ \mu\text{m}$

The fibre-MOPA (labelled laser "A" in this paper) consists of an oscillator, mode-locked by a SESAM (Semiconductor Saturable Absorber), and two amplification stages. Here, the oscillator generates laser pulses at a wavelength of $\lambda = 1965\ \text{nm}$ with a repetition rate of $f = 7.6\ \text{MHz}$, a pulse duration of $\tau_p = 2\ \text{ps}$ and a pulse energy of $W = 0.1\ \text{nJ}$. By using a pre-amplifier this pulse energy is amplified to $W = 0.5\ \text{nJ}$. Finally, the pulse is amplified in a second amplifier to a pulse energy of $W = 980\ \text{nJ}$ [32].

2. Ho-fibre based laser at $\lambda = 2090\ \text{nm}$

For experiments at 2090 nm we used a compact ultra-short pulsed fibre laser based Ho:YAG amplifier system from ATLA Lasers AS. At 10 kHz repetition rate the system delivered up to 760 μJ pulses with 5 ps duration from the amplifier stage. This laser system was used both with 500 fs-pulses and 5 ps-pulses, but in this paper we present only the results from the longer ps-pulses.

3. Er-fibre based Cr:ZnS laser at $\lambda = 2350\ \text{nm}$

The Er-based fibre laser (labelled laser "C" in this paper) was a mode-locked Cr:ZnS oscillator from ATLA Lasers AS working in the normal dispersion regime [33], pumped by the Er:fiber laser. The combination of dispersion-managed mirrors and material dispersion compensation in the cavity ensured the normal-dispersion operation regime of the laser. The laser generated linearly chirped pulses centred at 2350 nm with a duration of about $\tau_p = 1.7\ \text{ps}$ and pulse energy up to 48 nJ at a pulse repetition rate of 3.8 MHz. Around 50% of the pulse energy was lost in the isolator, beam delivery optics and focusing objective, resulting in slightly above 20 nJ delivered to a surface of a silicon sample.

B. Experimental setup

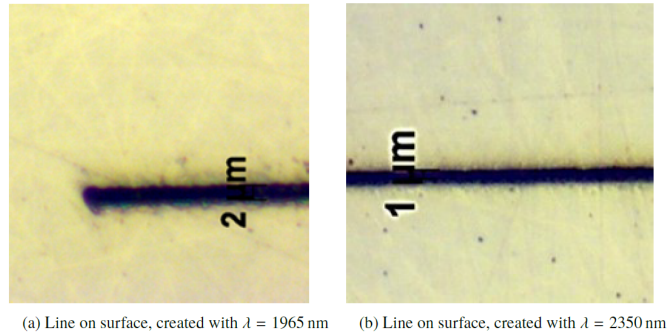
All lasers were coupled to a processing stage. The light was focused using an aspheric lens with varying focal distances, typically $f = 4\ \text{mm}$ either onto the surface of the sample (as in Figure 4) or inside the sample (as e.g. in Figure 7b). The sample itself was mounted onto a four-axis stage, with two axes controlled by an electronic controller. Electronic control allowed precise movement with a fixed speed, variable between several $\mu\text{m s}^{-1}$ and several mm s^{-1} . The sample itself was made out of monocrystalline silicon.

C. Investigation of the processed samples

The processed samples were investigated using three different techniques, including optical microscopy, transmission IR microscopy and scanning electron microscopy (SEM). The first two techniques are non-destructive, while the cross-sectional imaging using the SEM required splitting of the sample. Optical microscopy alone is applicable to study of the surface, while transmission IR microscopy was used to look through the sample and investigate sub-surface modifications without damaging the sample. As mentioned in Section I, both surface and sub-surface silicon modifications were created using pulses at both nJ and μJ pulse energy levels. In the first part of this section (Section IV C 1) the modifications created by pulses at sub- μJ pulse energy levels are investigated. In the second part (Section IV C 2) we investigate the modifications created by pulses with energies above 1 μJ .

1. Silicon modifications created at nJ pulse energy levels

We used the Tm-fibre-MOPA (laser A), operating at $f = 7.6\ \text{MHz}$ and $W = 28\ \text{nJ}$, and the Er-based fibre laser, operating at $\lambda = 2350\ \text{nm}$, $f = 3.7\ \text{MHz}$ and $W = 17\ \text{nJ}$ (laser C), to create modifications both on the surface and below the surface at nJ pulse energy levels. As initial test we created lines on the surface of the silicon sample, which directly could be observed with an optical microscope.



(a) Line on surface, created with $\lambda = 1965\ \text{nm}$ (b) Line on surface, created with $\lambda = 2350\ \text{nm}$

FIG. 4: Lines on surface, created with $\lambda = 1965\ \text{nm}$ and $\lambda = 2350\ \text{nm}$ [10]

For comparison in Figure 4 the cut using the longer wavelength is significantly smaller in diameter (1 μm compared to 2 μm) and cleaner with less residual around the cut, thus suggesting that using a longer wavelength might be beneficial for cutting of Si.

This size reduction could originate from a smaller spot size. Assuming that the beam was focused perfectly onto the surface, the focal spot size for laser A was 4.25 μm , while for laser C the spot size was 1.6 μm . Furthermore, we assumed that the absorption for laser A was purely based on two-photon-absorption, and the absorption from laser C was purely based on three-photon-absorption. This

means that the effective spot size (if the threshold is reached for the whole Gaussian pulse) is $3\ \mu\text{m}$ for laser A, and $0.92\ \mu\text{m}$ for laser C. While the result for laser C is close to the measured width of the lines, the calculated effective spot size for laser A is significantly larger than the measured line width. This can be related to several things, such as an incorrectly measured beam width (the effective spot size can be reached for a beam width of $1.6\ \text{mm}$), or a higher modification threshold, thereby also reducing the effective spot size. None of these possibilities can be excluded based on existing data.

After we could confirm that we can create modifications at the surface of silicon, we have conducted also the sub-surface modifications in silicon. For this task the same lasers as mentioned above were used, with varying pulse energy levels. Those modifications were observed both using a transmission FTIR and an infrared microscope. The FTIR microscopy was carried out in transmission mode on a Bruker Hyperion 3000 microscope with a 64×64 pixel mercury-doped CdTe focal plane array detector interfaced to a Bruker Vertex 70v FTIR spectrometer. A $10\times$ Cassegrain objective was used for imaging. Background spectral images were recorded on an empty sample stage and used to calculate extinction spectra at each pixel after measuring the laser processed Si sample. For spectral acquisition, 100 scans with a spectral resolution of $4\ \text{cm}^{-1}$ were averaged. Spectral images were obtained from two spectral regions. Extinction maps from the region $3.965 - 3.027\ \mu\text{m}$ ($2522 - 3304\ \text{cm}^{-1}$) were obtained as false-coloured maps from integrating extinction without baseline correction. As the system does not show any absorption in this spectral range, extinction here is caused by scattering. Maps were also produced in the spectral region $10.320 - 7.553\ \mu\text{m}$ ($969 - 1324\ \text{cm}^{-1}$), containing the absorption peaks of Si-O stretching modes. In this region, a linear baseline was subtracted from the spectra between the left and the right end of the spectral range. In that manner, maps show the distribution of absorption from Si-O modes. Results of those measurements for the laser operating at $1965\ \text{nm}$ (laser A) and for the laser operating at $2350\ \text{nm}$ (laser C) are displayed in Figures 5 and 6.

2. Silicon modifications created at μJ pulse energy levels

By using laser B operating at $\lambda = 2090\ \text{nm}$, we increased the pulse energy to several μJ . We used this increased pulse energy for creating larger sub-surface modifications, and investigated their shape afterwards. In addition, for faster non-destructive detection of sub-surface modifications in bulk silicon (compared to the FTIR used in Section IV C 1) we designed a special transmission IR-microscope operating at $\lambda = 1300\ \text{nm}$. To increase the modifications' visibility, the sample was moved parallel to the beam, while the samples shown in Figures 5 and 6 were moved perpendicular to the laser beam. This movement resulted in visible spots at the surface of the sample, shown in Figure 7a.

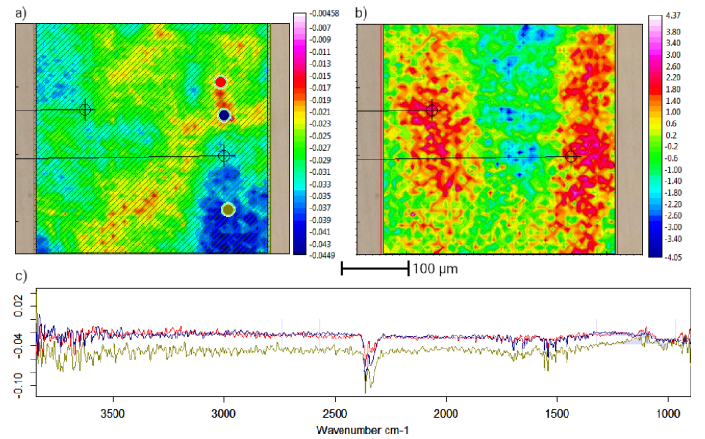


FIG. 5: Transmission IR images of a line below the surface of Si created with laser A operating at $\lambda = 1965\ \text{nm}$ and $W = 180\ \text{nJ}$. a) Mapped integrated extinction in the range $3.965 - 3.027\ \mu\text{m}$; b) mapped integrated absorbance in the region $10.320 - 7.553\ \mu\text{m}$. The scale bar applies to both a) and b). c) Example spectra at the spots marked in the respective colour in a). As in Figure 6, the continuation of the sample is shown as a visible image outside the IR maps.

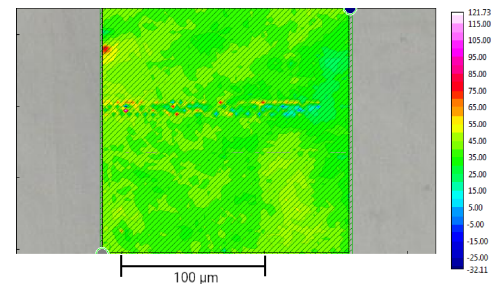


FIG. 6: Transmission IR image of a line created by focusing laser C with $\lambda = 2350\ \text{nm}$ below the surface of silicon. Right: False colored absorbance scale in the wavelength range $3.965 - 3.027\ \mu\text{m}$. The visible part of the image left and right of the central false coloured image presents a continuation in the visible of the area imaged in the IR. No modification is visible there, thus indicating that the modification resulting in increased absorption only exists below the surface.

The focal spot within the sample was moved vertically with a speed between $0.2 - 20\ \mu\text{m s}^{-1}$ from the bottom of the sample towards the top surface, while the pulse energy was varied between $3.7 - 7.7\ \mu\text{J}$. A side view of a part of the sample is shown in Figure 7b.

A second sample translated perpendicular to the beam using the same parameters is shown in Figures 8 to 10. Each line is marked, with the marks in Figures 8 and 9 and Figure 10 corresponding to each other.

There are modifications below the surface between line M4 and M6, even though they are not continuous. It also must be noted that lines M4, M5 and M6 are stacked lines,

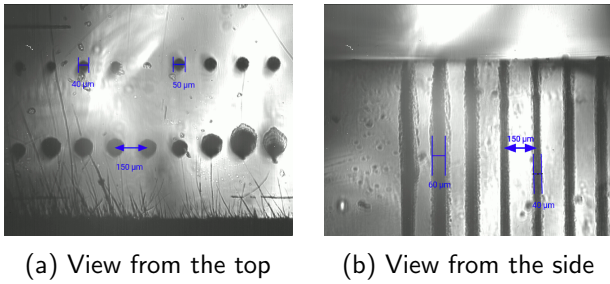


FIG. 7: Vertical lines, viewed using a transmission IR microscope from the top of the sample (Figure 7a) and the side of the sample (Figure 7b). The pulse energy was $3.7 \mu\text{J}$ and $7.7 \mu\text{J}$. The movement speed of the stage decreases from left to right.

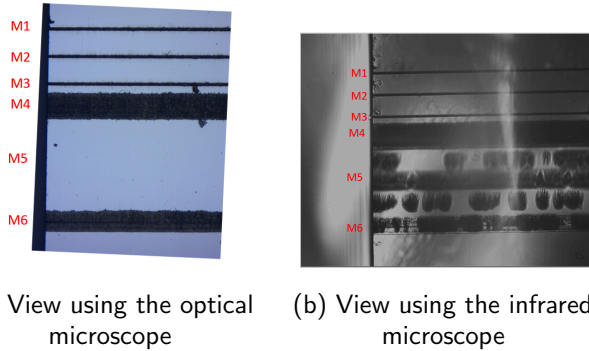


FIG. 8: View of the surface of the sample, using the optical microscope, and through the sample, using an infrared microscope.

i.e. several lines were drawn on top of each other. This "line-stacking" can also be seen when rotating the sample and watching it from the side using the IR microscope, as shown in Figure 9. After confirming that modifications below the surface were made, the sample was cleaved, and the cross section was investigated by SEM. The sample had to be observed from both sides, due to the spottiness of the lines. The different views from both sides are shown in Figure 10. It clearly can be seen that only a part of the observed modifications are visible on each side of the

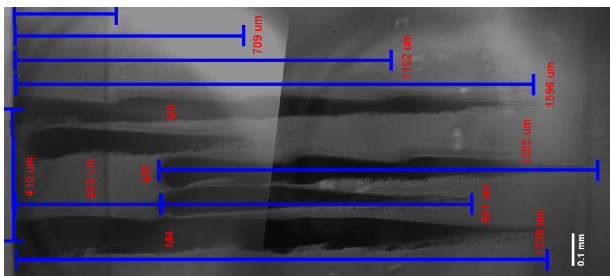


FIG. 9: Horizontal lines created in Si, watched from the side. Line stacking clearly is visible

sample, as for example line M6 from Figure 9. This line is only visible on the front side, but not on the back side. On the contrary, line M5 is visible on both sides.

When comparing Figure 9 with Figure 10, it can be also noted that the depths of the modifications are approximately equal, thereby indicating that the modifications observed in Figure 9 are the same as in Figure 10, even though the modifications visible in Figure 9 are larger than the modifications seen in Figure 10. Another fact worth mentioning is the shape of the modifications. Even though the beam was focused to a certain depth, the modifications started already significantly earlier, leading to elongated shapes. This broadening will be discussed in Section V.

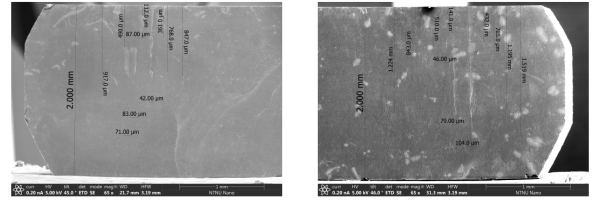


FIG. 10: SEM image of the sample surface. The left figure shows the front side of the sample, the right figure the back side of the sample

D. Summary

We showed three different lasers operating at central wavelengths of 1965-2350 nm and two different levels of pulse energies (nJ and μJ) and the resulting modifications of silicon both on the surface and below. The modifications were investigated in some more detail for $\lambda = 2090 \text{ nm}$, which we identified as a "sweet spot" for silicon modifications. The sub-surface modifications we generated with this laser could be visualised both by a custom-built transmission IR microscope and a SEM. The structures visible with both methods correlated in size. Sub-wavelength feature size was evidenced in Figure 4, but could not be observed yet for sub-surface structures as in Figures 7 to 10. A possible reason for that is the nonlinear absorption, which is starting already before the focal spot, thereby creating modifications with sizes larger than the laser wavelength as shown in the numerical simulation in Figure 2, and in the experiment in Figures 7 to 10.

V. DISCUSSION

As it can be seen in Figure 9 and other figures the created shapes within Si are not perfectly shaped around the focal spot, but rather elongated and start significantly before the focal spot. One possible explanation for that is that nonlinear absorption happens already earlier, i.e. the

critical intensity for material modification is reached already before the focal spot, starting the modification process before reaching the focal point. A similar behaviour is shown in Figure 2. One would expect the intensity to rise to one single peak, but instead it hits a maximum value, before staying at that level for several micrometres and decreasing again afterwards. In that period the pulse energy is absorbed within the material, and, depending on the pulse energy, is leading to modifications at points which are not targeted. This modified area also depends on the value for the non-linear Kerr value (as it can be seen in Figure 2a compared to Figure 2b for 1 μ J, and similarly in Figure 2c and Figure 2d for 10 μ J). The exact length of the modified area does not only depend on the pulse energy, but also on the value of the Kerr-coefficient.

This also means that a higher Kerr coefficient allows processing of Si at lower pulse energies. Lower energies will result in lower absorption on the way to the focal spot, while the self-focusing will occur later, and thereby resulting in a smaller modified area, which in turn explains the sub-surface modifications shown in Figure 5 and Figure 6. Both modifications were made at power levels significantly below 1 μ J, and thereby unable to damage the surface, while still modifying material below the surface.

Similar results are also reported by [15], which reported a lower threshold of 300 nJ for creating sub-surface modifications in Silicon when applying multiple pulses at the same spot. Finally, their reported fluence distribution matches the shape of the lines showed in fig. 9, which thereby confirms their simulations with experimental data.

VI. CONCLUSIONS

In this paper we investigated how the wavelength of the used laser influences the generated modifications at the surface and within silicon. This was done in three separate steps. On the one hand, we used a simple numerical model which included the wavelength dependency of the non-linear refractive index and the multi-photon absorption values, in Section III. On the other hand, we investigated the generation of modifications at two different pulse energy levels, at nJ and at μ J levels, with varying wavelengths.

As main conclusion of our results we can say that there is an optimal wavelength around 2.1 μ m where subsurface processing of Si occurs at comparatively low pulse energies.

Moreover, a few additional conclusions can be drawn. For example, for certain illumination parameters no visible damage on the surface was observed, but IR images showed a contrast in the volume of the material. Other groups experienced difficulties producing modifications inside the silicon volume without damaging the surface [34]. This knowledge can be used not only for creating a weakened layer below the surface, but also for creating wave guides. When comparing the pulse parameters given in [16, 34–38], sub-surface modifications here were created at comparable or lower pulse energies. Consequently, modifications at longer wavelengths ≥ 1550 nm, especially between 2000 nm and 2200 nm, have a lower damage threshold than at shorter and longer wavelengths, as predicted in Section III, and also confirmed in [15].

An increase of the pulse energy does not necessarily improve the processing; in some cases, it rather worsens the quality of the written structure by increasing the area where material is modified, though this could also be related to being the first results, which will need further improvement. In future studies we plan to apply a "burst pulse" approach and see if we can achieve improvements at both higher repetition rates and higher pulse energies per spot.

As an outlook, due to the non-linear behaviour of multi-photon absorption, it is possible to create structures with a characteristic size below the diffraction limit, something which is not easily achievable through direct writing with single-photon absorption. Additionally, it was possible with this method to create modified 2d-layers buried within the bulk silicon, something which, to the best of our knowledge, has not been reported before. This will be the subject of an upcoming publication.

The exact nature of the modified Si must be investigated in the future in more detail on the physical-chemical level in order to gain a better insight, and to improve the process. Still, the already achieved first results are quite promising, and further research has to be done at the wavelengths above 2 microns.

ACKNOWLEDGEMENTS

We would like to thank Prof. Patrick Espy very much for proofreading this work. This work was supported by ATLA Lasers AS, the Research Council of Norway - EN-ERGIX project #255003, as well as the Austrian Science Fund project #P24916 and COST Action MP1401. V.L.K. acknowledges the support by the Marie S.-Curie Cofund Multiply "MASTEDIS" Fellowship.

[1] F. Dross, K. Baert, T. Bearda, J. Deckers, V. Depauw, O. El Daif, I. Gordon, A. Gougam, J. Govaerts, S. Granata, R. Labie, X. Loozen, R. Martini, A. Masolin, B. O'Sullivan, Y. Qiu, J. Vaes, D. Van Gestel, J. Van Hoeymissen, A. Vanleenhove, K. Van Nieuwenhuysen,

S. Venkatachalam, M. Meuris, and J. Poortmans, "Crystalline thin-foil silicon solar cells: where crystalline quality meets thin-film processing," *Progress in Photovoltaics: Research and Applications*, vol. 20, no. 6, pp. 770–784, sep 2012. [Online]. Available:

- <http://doi.wiley.com/10.1002/PIP.1238>
- [2] M. Bruel, "Silicon on insulator material technology," *Electronics Letters*, vol. 31, no. 14, p. 1201, 1995. [Online]. Available: https://digital-library.theiet.org/content/journals/10.1049/el_{_}19950805
 - [3] H.-S. Lee, J. Suk, H. Kim, J. Kim, J. Song, D. Jeong, J.-K. Park, W. Kim, D.-K. Lee, K. Choi, B.-K. Ju, T. Lee, and I. Kim, "Enhanced efficiency of crystalline Si solar cells based on kerfless-thin wafers with nanohole arrays," *Scientific Reports*, vol. 8, no. 1, pp. 1–12, 2018. [Online]. Available: <http://dx.doi.org/10.1038/s41598-018-21381-2>
 - [4] Y. H. Lee, H. Cha, S. Choi, H. S. Chang, B. Jang, and J. Oh, "Characterization of Atomic-Layer-Deposited (ALD) Al₂O₃-Passivated Sub-50- μ m-thick Kerf-less Si Wafers by Controlled Spalling," *Electronic Materials Letters*, vol. 14, no. 3, pp. 363–369, 2018. [Online]. Available: <https://doi.org/10.1007/s13391-018-0039-9>
 - [5] S. Kajari-Schröder, J. Käsewiter, J. Hensen, and R. Brendel, "Lift-off of free-standing layers in the kerfless porous silicon process," in *Energy Procedia*, vol. 38, 2013, pp. 919–925.
 - [6] P. C. Verburg, "Laser-induced subsurface modification of silicon wafers," Ph.D. dissertation, University of Twente, Enschede, The Netherlands, 2015. [Online]. Available: <http://purl.org/utwente/doi/10.3990/1.9789036538381>
 - [7] A. Rämmer, O. Osmani, and B. Rethfeld, "Laser damage in silicon: Energy absorption, relaxation, and transport," *Journal of Applied Physics*, vol. 116, no. 5, 2014.
 - [8] A. Lietoila and J. F. Gibbons, "Computer modeling of the temperature rise and carrier concentration induced in silicon by nanosecond laser pulses," *Journal of Applied Physics*, vol. 53, no. 4, pp. 3207–3213, 1982. [Online]. Available: <https://doi.org/10.1063/1.331020>
 - [9] P. C. Verburg, G. R. B. E. Römer, and A. J. Huis in 't Veld, "Two-temperature model for pulsed-laser-induced subsurface modifications in Si," *Applied Physics A*, vol. 114, no. 4, pp. 1135–1143, mar 2014. [Online]. Available: <http://link.springer.com/10.1007/s00339-013-7668-5>
 - [10] R. A. Richter, N. Tolstik, and I. T. Sorokina, "In-bulk silicon processing with ultrashort pulsed lasers: Three-photon-absorption versus two-photon-absorption," in *High-Brightness Sources and Light-driven Interactions*. Washington, D.C.: OSA, 2018, p. MW4C.2. [Online]. Available: <http://www.osapublishing.org/abstract.cfm?URI=MICS-2018-MW4C.2https://www.osapublishing.org/abstract.cfm?URI=MICS-2018-MW4C.2>
 - [11] E. V. Zavedeev, V. V. Kononenko, and V. I. Konov, "Delocalization of femtosecond laser radiation in crystalline Si in the mid-IR range," *Laser Physics*, vol. 26, no. 1, p. 16101, 2016. [Online]. Available: <http://stacks.iop.org/1555-6611/26/i=1/a=016101?key=crossref.4797a52086849cbe611dae05222aeca2>
 - [12] M. Kumagai, N. Uchiyama, E. Ohmura, R. Sugiura, K. Atsumi, and K. Fukumitsu, "Advanced dicing technology for semiconductor wafer - Stealth Dicing," *IEEE International Symposium on Semiconductor Manufacturing Conference Proceedings*, vol. 20, no. 3, pp. 215–218, 2006.
 - [13] D. P. Korfiatis, K. A. T. Thoma, and J. C. Vardaxoglou, "Conditions for femtosecond laser melting of silicon," *Journal of Physics D: Applied Physics*, vol. 40, no. 21, pp. 6803–6808, 2007.
 - [14] Y. Gan and J. K. Chen, "Combined continuum-atomistic modeling of ultrashort-pulsed laser irradiation of silicon," *Applied Physics A*, vol. 105, no. 2, pp. 427–437, nov 2011. [Online]. Available: <http://link.springer.com/10.1007/s00339-011-6573-z>
 - [15] M. Chambonneau, L. Lavoute, D. Gaponov, V. Fedorov, A. Hideur, S. Février, S. Tzortzakis, O. Utéza, and D. Grojo, "Competing Nonlinear Delocalization of Light for Laser Inscription Inside Silicon with a 2- μ m Picosecond Laser," *Physical Review Applied*, vol. 12, no. 2, p. 1, 2019. [Online]. Available: <https://doi.org/10.1103/PhysRevApplied.12.024009>
 - [16] A. H. Nejadmalayeri, P. R. Herman, J. Burghoff, M. Will, S. Nolte, and A. Tünnermann, "Inscription of optical waveguides in crystalline silicon by mid-infrared femtosecond laser pulses," *Optics Letters*, vol. 30, no. 9, p. 964, 2005. [Online]. Available: <http://ol.osa.org/abstract.cfm?URI=ol-30-9-964>
 - [17] H. O. Jeschke, M. E. Garcia, M. Lenzner, J. Bonse, J. Krüger, and W. Kautek, "Laser ablation thresholds of silicon for different pulse durations: Theory and experiment," *Applied Surface Science*, vol. 197–198, pp. 839–844, 2002.
 - [18] B. N. Chichkov, C. Momma, S. Nolte, F. Von Alvensleben, and A. Tünnermann, "Femtosecond, picosecond and nanosecond laser ablation of solids," *Applied Physics A: Materials Science and Processing*, vol. 63, no. 2, pp. 109–115, 1996.
 - [19] Q. Lin, J. Zhang, G. Piredda, R. W. Boyd, P. M. Fauchet, and G. P. Agrawal, "Dispersion of silicon nonlinearities in the near infrared region," *Applied Physics Letters*, vol. 91, no. 2, pp. 2–4, 2007.
 - [20] T. Wang, N. Venkatram, J. Gosciniak, Y. Cui, G. Qian, W. Ji, and D. T. H. Tan, "Multi-photon absorption and third-order nonlinearity in silicon at mid-infrared wavelengths," *Optics express*, vol. 21, no. 26, pp. 32 192–32 198, 2013. [Online]. Available: <http://www.ncbi.nlm.nih.gov/pubmed/24514813>
 - [21] V. Mizrahi, M. A. Saifi, M. J. Andrejco, K. W. DeLong, and G. I. Stegeman, "Two-photon absorption as a limitation to all-optical switching," *Optics Letters*, vol. 14, no. 20, p. 1140, 1989. [Online]. Available: <https://www.osapublishing.org/abstract.cfm?URI=ol-14-20-1140>
 - [22] F. Gholami, S. Zlatanovic, A. Simic, L. Liu, D. Borlaug, N. Alic, M. P. Nezhad, Y. Fainman, and S. Radic, "Third-order nonlinearity in silicon beyond 2350 nm," *Applied Physics Letters*, vol. 99, no. 8, pp. 1–4, 2011.
 - [23] D. Arndt, W. Bangerth, T. C. Clevenger, D. Davydov, M. Fehling, D. Garcia-Sanchez, G. Harper, T. Heister, L. Heltai, M. Kronbichler, R. M. Kynch, M. Maier, J.-P. Pelteret, B. Turcksin, and D. Wells, "The deal.II library, version 9.1," *Journal of Numerical Mathematics*, 2019, accepted. [Online]. Available: <https://dealii.org/deal91-preprint.pdf>
 - [24] S. Nemoto, "Nonparaxial Gaussian beams," *Applied Optics*, vol. 29, no. 13, p. 1940, 1990. [Online]. Available: <https://www.osapublishing.org/abstract.cfm?URI=ao-29-13-1940>
 - [25] B. Rethfeld, D. S. Ivanov, M. E. Garcia, and S. I. Anisimov, "Modelling ultrafast laser ablation," *Journal of Physics D: Applied Physics*, vol. 50, no. 19, p. 193001, 2017. [Online]. Available: <http://stacks.iop.org/0022-3727/50/i=19/a=193001?key=crossref.018ba9a682d87e828aa07398bc0c13af>
 - [26] S. H. Lee, H. S. Sim, J. Lee, J. M. Kim, and Y. E. Shin, "Three Temperature Model for Nonequilibrium Energy

- Transfer in Semiconductor Films Irradiated with Short Pulse Lasers,” *Materials Transactions*, vol. 47, no. 11, pp. 2835–2841, 2006.
- [27] D. Perez and L. J. Lewis, “Molecular-dynamics study of ablation of solids under femtosecond laser pulses,” *Physical Review B - Condensed Matter and Materials Physics*, vol. 67, no. 18, pp. 1–15, 2003.
- [28] T. Zier, E. S. Zijlstra, A. Kalitsov, I. Theodonis, and M. E. Garcia, “Signatures of nonthermal melting,” *Structural Dynamics*, vol. 2, no. 5, p. 54101, 2015. [Online]. Available: <http://dx.doi.org/10.1063/1.4928686><http://aca.scitation.org/doi/10.1063/1.4928686>
- [29] K. Sokolowski-Tinten and D. von der Linde, “Generation of dense electron-hole plasmas in silicon,” *Physical Review B*, vol. 61, no. 4, pp. 2643–2650, jan 2000. [Online]. Available: <https://link.aps.org/doi/10.1103/PhysRevB.61.2643>
- [30] C. V. Shank, R. Yen, and C. Hirlimann, “Femtosecond-time-resolved surface structural dynamics of optically excited silicon,” *Physical Review Letters*, vol. 51, no. 10, pp. 900–902, 1983.
- [31] P. Stampfli and K. H. Bennemann, “Dynamical theory of the laser-induced lattice instability of silicon,” *Physical Review B*, vol. 46, no. 17, pp. 10 686–10 692, 1992.
- [32] R. A. Richter, N. Tolstik, and I. T. Sorokina, “1 uJ pulse energy all-fiber thulium doped mode-locked mopa system,” in *2019 Conference on Lasers and Electro-Optics Europe and European Quantum Electronics Conference*. Optical Society of America, 2019, p. cj.p.13. [Online]. Available: http://www.osapublishing.org/abstract.cfm?URI=CLEO_Europe-2019-cj_p.13
- [33] N. Tolstik, C. S. J. Lee, E. Sorokin, and I. T. Sorokina, “8.6 MHz extended cavity Cr:ZnS chirped-pulse oscillator,” *2018 Conference on Lasers and Electro-Optics, CLEO 2018 - Proceedings*, pp. 1–2, 2018.
- [34] P. V. V. Sreenivas, M. B. Ülters, and R. B. Bergmann, “Microsized subsurface modification of mono-crystalline silicon via non-linear absorption,” *Journal of the European Optical Society*, vol. 7, pp. 3–7, 2012.
- [35] Y. Izawa, S. Tanaka, H. Kikuchi, Y. Tsurumi, N. Miyanaga, M. Esashi, and M. Fujita, “Debris-free in-air laser dicing for multi-layer MEMS by perforated internal transformation and thermally-induced crack propagation,” *Proceedings of the IEEE International Conference on Micro Electro Mechanical Systems (MEMS)*, pp. 822–827, 2008.
- [36] O. Tokel, A. Turnall, G. Makey, P. Elahi, T. Çolakolu, E. Ergeçen, Ö. Yavuz, R. Hübner, M. Zolfaghari Borra, I. Pavlov, A. Bek, R. Turan, D. K. Kesim, S. Tozburun, S. İlday, and F. Ö. İlday, “In-chip microstructures and photonic devices fabricated by nonlinear laser lithography deep inside silicon,” *Nature Photonics*, vol. 11, no. 10, pp. 639–645, 2017. [Online]. Available: <http://dx.doi.org/10.1038/s41566-017-0004-4>
- [37] I. Pavlov, O. Tokel, S. Pavlova, V. Kadan, G. Makey, A. Turnali, Ö. Yavuz, and F. Ö. İlday, “Femtosecond laser written waveguides deep inside silicon,” *Optics Letters*, vol. 42, no. 15, p. 3028, 2017. [Online]. Available: <https://www.osapublishing.org/ol/fulltext.cfm?uri=ol-42-15-3028&id=370248%0Ahttps://www.osapublishing.org/abstract.cfm?URI=ol-42-15-3028>
- [38] H. Kämmer, G. Matthäus, S. Nolte, M. Chanal, O. Utéza, and D. Grojo, “In-volume structuring of silicon using picosecond laser pulses,” *Applied Physics A*, vol. 124, no. 4, p. 302, apr 2018. [Online]. Available: <http://link.springer.com/10.1007/s00339-018-1715-1>